様式①

【研究成果の要約】

氏　名	藤原　翔
1. 研究題目	燃焼合成法による環境浄化用 Ag クラスター触媒の開発

2. 研究内容

本研究は排ガス処理（CO 等の有害物質分解）に高い活性を示す Ag 微粒子触媒の開発を試みた。一般的に Ag は融点が低いため，200～300℃で粒子同士の焼結による粒子サイズ増大が避けられない。このため触媒活性が高い Ag 微粒子（～2 nm）は反応中に粒子サイズが増加してしまい，触媒活性が低下する。そこで Strong metal-support interaction （SMSI）と呼ばれる Ag と酸化物担体の間で発現する相互作用により，Ag 微粒子（～2 nm）の安定化を試みた。この相互作用が Ag 微粒子（～2 nm）の安定化することは既往研究で報告済みであるが，その触媒活性は不明であった。また Ag/TiO_2 系以外で同様の相互作用が発現するかは不明である。

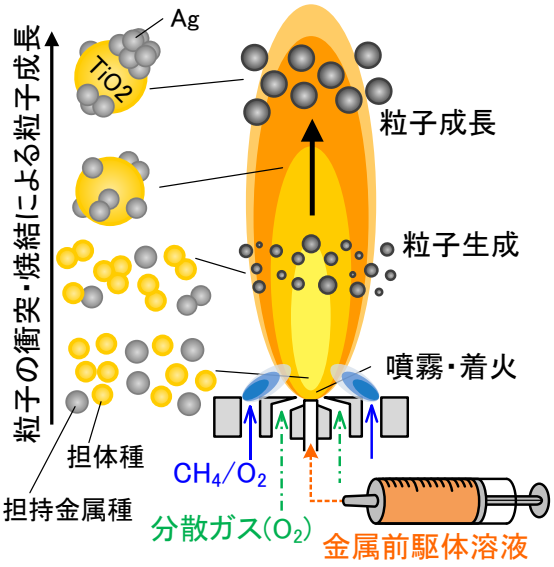

Fig. 1 FSP 反応器による Ag 触媒の合成

そこで Fig.1 に示す火炎噴霧熱分解法を用いて，Ag と様々な酸化物担体（SiO_2, Al_2O_3, ZrO_2, CeO_2）を組み合わせた場合，触媒性能がどのように変化するかを検討した。また TiO_2 以外の酸化物においても燃焼反応によって相互作用が発現するかを調査した。触媒材料は酢酸銀と各酸化物の原料（Ti イソプロポキシド，オルトケイ酸テトラエチル，硝酸 Al 九水和物，Zr イソプロポキシド，硝酸 Ce 六水和物）を溶解した有機溶媒（メタノール + 2-エチルヘキサン酸）を FSP 反応器で燃焼して合成した。触媒中に含まれる Ag 量が 20wt.%となるよう，酢酸銀と各酸化物の原料を混合した。得られた Ag 触媒は 350℃で2時間空気焼成を行った後，固定床流通反応器で CO 酸化反応活性を評価した。

3. 研究成果

合成した触媒の CO 転化率（＝反応した CO 量÷供給した CO 量）を Fig.2 に示す。Ag 触媒の活性は組み合わせた酸化物担体によって大きく異なり，TiO_2, CeO_2, ZrO_2, Al_2O_3, SiO_2 の順に高かった。SMSI 発現を示す亜酸化物（例えば TiO_x, $x < 2$）の生成を X 線回折法により調査したところ TiO_2 以外の担体では亜酸化物は生成しないことが判明した。

TiO_2 と組み合わせた Ag 触媒が高活性である要因について各種分光法で調査した結果、Ag の電子状態が反応性の高い Ag^+であることが判明した。Ag の電子状態および相互作用で生成した TiO_x は、CO 酸化反応前後で変化せず安定であることも見出した。

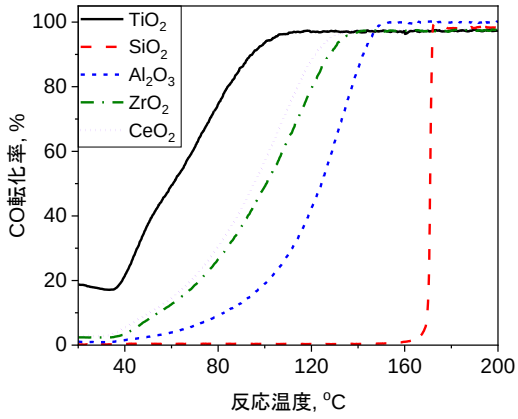

Fig. 2 FSP 法で合成した Ag 触媒による CO 酸化反応（1%CO+19%O_2+N_2）の活性に担体種が与える影響

様式②

【研究成果の概要】

氏　名	藤原　翔
1. 研究題目	燃焼合成法による環境浄化用 Ag クラスター触媒の開発

別添の発表予定論文をご確認ください。

Ag clusters on titanium oxides under metal–support interactions for the catalytic oxidation of CO at room temperature

by

Kakeru Fujiwara[1, 2*], Souki Terazawa[2], Masahiko Nishijima[3], Yugo Osaka[4], Takuya Tsujiguchi[4] and Akio Kodama[1]

1. Institute for Frontier Science Initiative, Kanazawa University, Kakuma-machi, Kanazawa, Ishikawa 920-1192, Japan.
2. Department of Chemistry and Chemical Engineering, Yamagata University, 4–3–16 Jonan, Yonezawa, Yamagata 992-8510, Japan.
3. Flexible 3D System Integration Lab, SANKEN, Osaka University, 8–1 Mihogaoka, Ibaraki, Osaka 567-0047, Japan.
4. Faculty of Mechanical Engineering, Institute of Science and Engineering, Kanazawa University, Kakuma-machi, Kanazawa, Ishikawa, 920-1192, Japan.

*Corresponding author: k-fujiwara@staff.kanazawa-u.ac.jp

Abstract

Silver-loaded titanium oxide catalysts (*m* wt% Ag on TiO_2, *m*FSP) were synthesized via flame spray pyrolysis (FSP) and evaluated for their abilities to oxidize CO. X-ray diffraction and X-ray photoelectron spectroscopy revealed that the FSP-prepared catalysts (*m*FSP) contained sub-stoichiometric TiO_x ($x < 2$), which was formed through interactions between titanium oxides and Ag during FSP synthesis. These interactions led to the formation of cationic Ag, as confirmed by X-ray photoelectron and Auger electron spectroscopies. Furthermore, these interactions suppress the sintering of small Ag clusters (< 3 nm). The small Ag size and cationic oxidation state induced by these interactions enhanced catalytic activity. The FSP-based catalysts exhibited higher CO oxidation activities than a wet-prepared catalyst. In particular, 20FSP demonstrated 18% CO conversion at room temperature and maintained its catalytic activity over multiple cycles of use. The amounts of reactive oxygen species (ROS), which can proceed with oxidation reactions were evaluated using H_2 pulse titration. Notably, *m*FSP generated more ROS than the wet-made catalyst. Furthermore, while ROS can be regenerated by reacting *m*FSP with oxygen, the wet-made catalyst is not endowed with this ability. These findings demonstrate that unique flame-induced interactions are crucial for achieving high catalytic activity and durability. Flame spray pyrolysis is a promising method for the scalable production of efficient Ag catalysts.

Keywords

Flame spray pyrolysis, Flame synthesis, Metal–support interactions, TiO_x, Sub-stoichiometric oxide

1. Introduction

Volatile organic compounds (VOCs) and carbon monoxide (CO) are common air pollutants emitted by various industrial and domestic sources that pose serious environmental and health risks. Catalytic oxidation is among the most effective strategies for removing these compounds under mild conditions. [1, 2] Most room-temperature-active catalysts rely on expensive noble metals (e.g., Pt, Rh, Pd [3], and Au [4]), which limits their widespread use. Silver, a relatively inexpensive noble metal, has attracted considerable attention as a low-temperature oxidant owing to its unique redox properties and moderate cost. Room-temperature-effective Ag catalysts are expected to provide a cost-efficient alternative for use in passive air-purification systems.

The oxidation behavior of Ag catalysts for use in environmental-remediation applications has been studied on numerous occasions, with a focus on the relationship between activity and properties. Particle size is a key factor, with numerous studies showing that smaller Ag particles exhibit significantly higher CO oxidation activity. Furthermore, the turnover frequency for CO oxidation per surface Ag atom was found to increase with decreasing particle size for Ag particles less than 5 nm in size. [5] Lamoth et al. [6] demonstrated that the size of the Ag particles in a supported catalysts affects the strength of its Ag-O bonds, and catalytic activity as a consequence. Ag particle size is strongly influenced by interactions between Ag and the support. For instance, Dutov et al. [7, 8] reported that OH species on the SiO_2 surface stabilize Ag nanoparticles; as a result, the Ag becomes more dispersed as the OH/Ag ratio increases. Furthermore, oxygen-defect sites on the CeO_2 surface [9] and Lewis-acid sites on the Al_2O_3 surface [5] bind Ag particles. Such interactions between Ag and a support alter the oxidation state of the Ag, which plays a critical role in determining catalytic activity. Rod-shaped CeO_2, which contains numerous oxygen defects, strongly binds Ag_n^+ clusters; however, such Ag clusters are less active than Ag

nanoparticles. [10] In contrast, cationic Ag species (or Ag_2O) tend to be more oxidizing compared to metallic Ag. [11, 12] Zhang et al. suggested that there is an optimal $Ag^0/Ag^{\delta+}$ ratio that delivers the highest catalytic activity. [13] In addition, specific pretreatment conditions can alter Ag-particle crystallinity such that a polycrystalline state is formed, which contributes to improved catalytic performance. [14]

Despite extensive research, conventional catalysts rarely promote oxidation reactions at ambient temperatures [7, 9, 15], which highlights the critical need for further development. Furthermore, the relatively low Tammann temperature of Ag (344 °C [16]) suffers from the particle growth through agglomeration and sintering, resulting in fewer exposed active sites. Recently, we developed thermally stable Ag clusters (< 3 nm) supported on titanium oxide particles using flame spray pyrolysis (FSP). [17, 18] FSP is an aerosol process that can be scaled up to produce kilograms of particles per hour [19, 20]. The simultaneous formation of Ag and TiO_2 NPs in a flame generates unique metal–support interactions between titanium oxide and Ag particles that stabilize small metal clusters. [17] Furthermore, FSP can deposit highly dispersed metal clusters (e.g., Pd [21, 22], Pt [23], ZnO [24], and VO_x [25]) on metal oxide supports under relatively high loading conditions. Consequently, titanium oxide can support large amounts of thermally stable Ag clusters, which maximizes the content of highly active Ag clusters.

In this study, Ag-loaded TiO_2 catalysts (*m*FSP, m = 0–40 wt%) were synthesized via flame spray pyrolysis. For comparison, 10 wt% Ag was also deposited on Ag-free FSP-made TiO_2 (0FSP) using a conventional impregnation method (referred to as "10IMP"). The catalytic CO-oxidation activities of *m*FSP and 10IMP were evaluated in a fixed-bed reactor. The amount of reactive oxygen species, which correlates with catalytic activity, was evaluated using H_2 and O_2 pulse titration experiments.

The sizes of the Ag particles in the various catalysts were determined by electron microscopy. The

existence of Ag and titanium oxides and their interaction states were evaluated by powder X-ray diffraction (PXRD), X-ray photoelectron spectroscopy (XPS) and Auger electron spectroscopy (AES).

2. Materials and Methods

2.1 Catalyst preparation

Ag supported on titanium oxide was prepared by FSP. [17] Silver acetate (Fujifilm Wako Pure Chemical, purity > 99%) and titanium isopropoxide (Sigma–Aldrich, purity > 97%) were used as the Ag and Ti precursors, respectively. An appropriate amount of each precursor was dissolved in a 1:1 (v/v) mixture of 2-ethylhexanoic acid (Sigma–Aldrich, purity > 99%) and acetonitrile (Fujifilm Wako Pure Chemical, Guaranteed Reagent). The Ag loading was controlled by varying the Ag/Ti precursor ratio, while the total metal (Ti +Ag) concentration in the solution was fixed at 0.2 mol L^{-1}. The precursor solution was fed to the FSP reactor at 3 mL min^{-1}, and dispersed to fine droplets using O_2 (purity > 99.5 %) at 5 L_{STP} min^{-1}. The dispersed solution was ignited using a pilot flame composed of CH_4 (1.5 L_{STP} min^{-1}) and O_2 (3.2 L_{STP} min^{-1}). Combustion of the solution produced particles that were collected using a vacuum pump (Busch, Seco SV1040) and a glass fiber filter (Hahnemühle, GF6, 257 mm). The distance between the FSP nozzle and filter was set to 65 cm. The produced catalysts were calcined in air at 350 °C for 2 h to remove incomplete combustion products. Hereafter, these catalysts are referred to as "*m*FSP", where *m* is the mass percentage of the Ag in the catalyst, assuming that the composition is *m*Ag/TiO_2.

For comparison, 10 wt% Ag supported on commercial TiO_2 (10IMP) was prepared using an impregnation method. Here, silver acetate was dissolved in 100 mL of deionized water and the resulting solution was mixed with 0.5 g of TiO_2 powder (P25, Evonik) and stirred for 24 h. The mixture was dried using a rotary evaporator under vacuum (~0.3 bar) at 60 °C. The dried powder was grained and

subsequently calcined in air at 350 °C for 4 h.

2.2 Catalyst characterization

The prepared materials were characterized using powder PXRD, N_2-adsorption experiments, XPS, AES, and high-angle annular dark-field scanning transmission electron microscopy (HAADF-STEM). Details are provided in the Supporting Information.

2.3 Evaluating catalyst reactivity

The CO-oxidation activities of the catalysts were examined in a fixed-bed reactor. The catalyst (30 mg) and 1.0 g of quartz sand (Fujifilm Wako Pure Chemical, 20–35 mesh) were mixed and then placed in a quartz reactor (inner/outer diameters: 8/6 mm). The reactant gas ($CO/O_2/N_2$ = 1/19/80) was fed to the catalyst at 30 mL_{STP} min^{-1} (6×10^4 mL_{STP} h^{-1} g_{cat}^{-1}). The reaction temperature was measured using a K-type thermocouple (ϕ 1 mm) placed downstream of the catalyst bed. The temperature was ramped from 25 to 200 °C at 1 °C min^{-1}. The reaction product (CO_2) was quantified using a CO_2 meter (VAISALA, GMP252 12C0B0N1) with a flow-through adopter (ASM212011SP). CO conversion was evaluated using the following equation:

$$\text{CO conversion [\%]} = F_{CO2\_out} / F_{CO\_in} \times 100 \quad (1),$$

where F_{CO_in}, and F_{CO2_out} are the flow rates of CO (mol s^{-1}) at the inlet and CO_2 (mol s^{-1}) at the outlet, respectively.

The amount of reactive oxygen species (ROS) contained in the catalyst was evaluated via H_2 and O_2 pulse titration using a BELCAT II (MicrotracBEL Corp.). A quartz reactor was filled with 20 mg of the sample, which was then pretreated in 20% O_2 in N_2 at 350 °C for 1 h. The sample was subsequently

cooled to a specific temperature (100–200 °C). After the temperature had stabilized for 15 min, 0.097 mL_{STP} of H_2 was injected into 50 mL min^{-1} of Ar (50 mL min^{-1}, as the carrier) every 2 min until the H_2 was no longer consumed by the catalyst. H_2 consumption was assumed to follow the following reaction:

$$Ag_2O + H_2 \rightarrow Ag + H_2O \quad (2).$$

The reactive oxygen species in the sample were subsequently regenerated via O_2 pulse titration, in which O_2 (0.097 mL_{STP}) was injected into He (50 mL min^{-1}, as the carrier) every 2 min until O_2 was no longer consumed by the sample. H_2 pulse titration was then used to evaluate the amount of regenerated reactive oxygen species.

3. Results and Discussions

3.1 Catalytic activities of FSP-made Ag catalysts

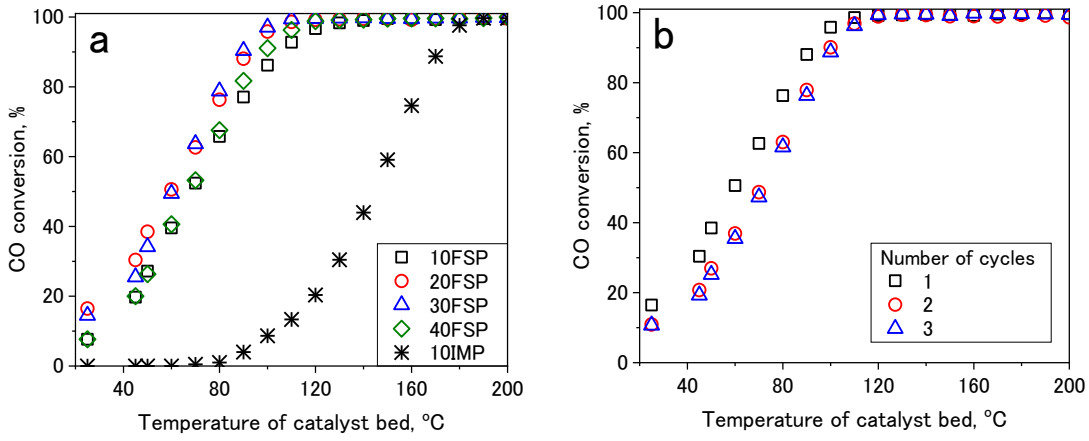

Figure 1 (a) CO-oxidation activities of *m*FSP (*m* = 10–40 wt%) and 10IMP, and (b) durability of the 20FSP catalyst during three reaction cycles.

The catalytic CO-oxidation performance of the FSP-made Ag clusters was examined. Figure 1 shows CO conversions for the *m*FSP (*m* = 0–40 wt%) and 10IMP catalysts. Notably, *m*FSP exhibited CO-oxidation activity at 25 °C, with 20FSP delivering a conversion of 16% at a relatively high gas feed rate (60 L_{STP} h^{-1} g_{cat}^{-1}). The highest conversions were achieved over 20FSP and 30FSP, which suggests that

20–30 wt% is the optimal Ag content. These catalysts (20FSP and 30FSP) delivered more than 95% CO conversion at 100 °C. In contrast, the wet-made catalyst (10IMP) exhibited a light-off temperature of around 80 °C, which is comparable with those of other reported Ag/TiO_2 catalysts. [26, 27] Therefore, the FSP-made Ag catalysts show superior oxidation activities than conventional Ag catalysts.

The catalytic durability of 20FSP was examined through repeated reactions in the 25–200 °C range. Figure 1b shows the CO conversion of 20FSP during three reaction cycles, which reveals that the second cycle delivered a slightly lower conversion than the first cycle, but it was identical to that observed in the third. Cyclic testing revealed that 20FSP is highly durable despite the slight performance degradation observed following the initial cycle.

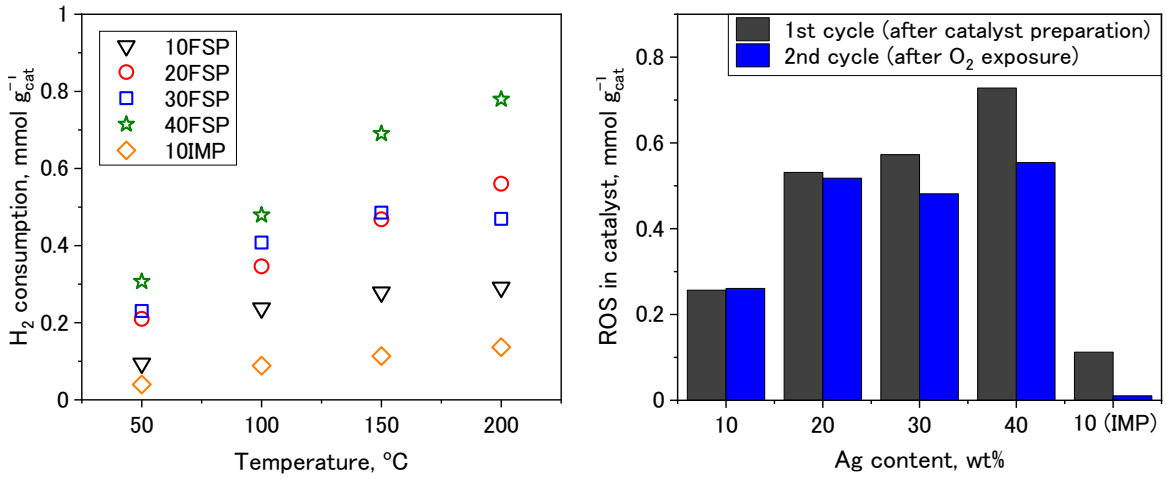

Figure 2 (a) Amounts of H_2 consumed by the catalysts as functions of temperature. (b) Amounts of reactive oxygen species (ROS) in the catalysts during the first (after catalyst preparation) and second (after ROS regeneration by exposure to O_2) cycles.

The oxidation activity of a Ag catalysts can be correlated with the amount of reactive oxygen species (ROS) produced by the catalyst. Accordingly, we evaluated, the ROS contents of the catalysts by H_2 pulse titration, in which the introduced H_2 reacts with ROS in the catalysts ($xH_2 + AgO_x \rightarrow Ag + xH_2O$);

consequently the amount of ROS is determined from the amount of consumed H_2.

Figure 2a shows the amounts of H_2 consumed by the *m*FSP and 10IMP as functions of temperature in the 50−200 °C range. H_2 consumption was observed to increase over each catalyst as the titration temperature was increased from 50 to 150 °C. Consumption was observed to plateau above 150 °C, which indicates that almost all of the ROS were consumed by H_2 at 150 °C. These ROS reaction-temperature profiles are consistent with observations of Seyedmonir et al. [28], who reported that ROS on the Ag surface had reacted with H_2 below 170 °C. Therefore, we evaluated the amount of ROS produced in each catalyst by titration at 150 °C.

The catalysts were exposed to O_2 via O_2 pulse titration at 150 °C following H_2 titration; this exposure regenerated ROS on the Ag surface. The amount of regenerated ROS was then evaluated by H_2 titration, the result of which are displayed in Fig. 2b. The ROS contents of the as-prepared *m*FSP catalysts (first cycle) were observed to increase with increasing Ag content. The regenerated ROS contents in the *m*FSP catalysts following O_2 exposure (second cycle) are comparable to those observed in the first cycle, with only 30FSP and 40FSP showing slightly lower values. In contrast, 10IMP produced significantly less ROS during the second cycle, which suggests that titration changes the structure of 10IMP and/or that the Ag in the 10IMP catalyst is not active toward molecular oxygen. The low stability and reactivity of 10IMP are attributable to its inferior CO-oxidation activity when compared to that of the *m*FSP series (Fig. 1a). Among the *m*FSP catalysts, 20FSP appears to contain the optimal amount of Ag because it produced the most ROS and was most stable when cycled.

3.2 Material properties of the FSP-made Ag–TiO_2 catalysts

CO-oxidation test and the pulse-titration experiments revealed that the FSP-prepared catalysts have

promising activities. Unique Ag/TiO_2 interactions formed when Ag–TiO_2 was synthesized by FSP, resulting in the formation of TiO_x (x < 2). [17] How these interactions affect catalytic activity were investigated by PXRD to determine the presence and stability of the TiO_x species.

PXRD patterns of *m*FSP and 10IMP are displayed in Fig. 3. Anatase TiO_2 is the major crystalline phase in 0FSP (devoid of Ag). The inclusion of Ag led to a metallic Ag peak at 44°, irrespective of the preparation method used (FSP*x* or IMP). In contrast, the PXRD patterns of the *m*FSP catalysts exhibited peaks that correspond to crystalline TiO_x ($x < 2$) at 29° and 33° [17], and their intensities were observed to increase with increasing Ag content. The positions of these peaks (29° and 33°) are similar to those of the bronze TiO_2 phase formed by FSP, [29] albeit with the characteristic peak at 15° ascribable to bronze TiO_2 absent in the PXRD patterns of 10–40FSP. Moreover, peaks corresponding to TiO_x were not observed in the PXRD pattern of 10IMP, the wet-prepared Ag/TiO_2. Therefore, we conclude that sub-stoichiometric TiO_x is formed via Ag–TiO_2 interactions as particles are produced in the flame. These interactions led to the formation of small Ag particles.

Ag crystallite sizes are listed in Table 1. When the Ag content was 10 wt%, the crystallite size of 10FSP was smaller than that of 10IMP. By increasing the Ag content. Notably, 40FSP contains smaller crystallites than 10IMP, despite it containing four-times the amount of Ag. It should be noted that the *m*FSP catalysts were calcined in 350 °C, which is above than Tammann temperature of bulk Ag (~344 °C) [16]. Therefore, interactions formed during flame synthesis strongly bind the Ag to the titanium oxide support, which suppresses Ag-particle sintering above the Tammann temperature. Additionally, the much larger surface area of *m*FSP compared to that of 10IMP is attributable to its small Ag particles.

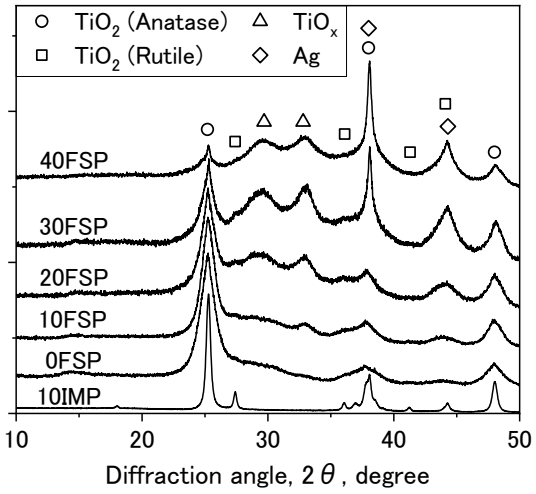

Figure 3 PXRD patterns of *m*FSP (*m* = 0−40 wt%) and 10IMP.

Table 1 Specific surface area (SSA) of each catalyst and its Ag crystallite size ($d_{XRD\text{-}Ag}$)

Catalyst	$d_{XRD\text{-}Ag}$, nm	SSA, $m^2\ g_{cat}^{-1}$
0FSP	N/A	209
10FSP	3	198
20FSP	4	164
30FSP	5	147
40FSP	7	120
10IMP	10	45

The stability of the Ag-TiO_2 interaction during the reaction was also examined. Figure 4 reveals that the PXRD patterns of 20FSP acquired before and after three reaction cycles are identical. For instance, the peaks for the TiO_x phases were equally intense before and after reaction. In addition, Ag crystallite size also remained unchanged, at 4 nm. Therefore, interactions within the *m*FSP sample remain stable during the reaction; these interactions are attributable to the highly active and durable catalytic activity of 20FSP, since they are only formed in the catalysts prepared by FSP.

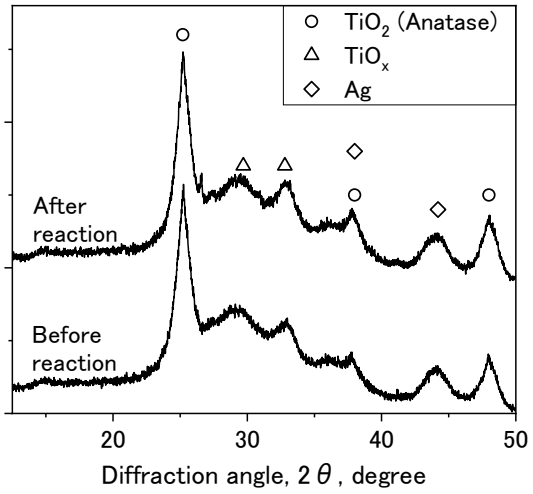

Figure 4 PXRD patterns of 20FSP before and after three reaction cycles.

The PXRD patterns in Fig. 3 suggest that the Ag crystallites in the *m*FSP samples are smaller than those in 10IMP. However, very small Ag clusters are not detectable by PXRD; consequently, the actual sizes of the Ag particle in the catalysts remain unclear. Hence, we used microscopic imaging to determine the sizes of the Ag particles. Figure 5 shows HAADF-STEM images of 20FSP, 40FSP, and 10IMP, with additional images provided in the Supporting Information (Fig. S1 and S2). 20FSP is predominantly composed of small Ag clusters (bright spots) deposited on titanium oxide particles (gray regions). Relatively large Ag particles (~10 nm) were observed to dominate as the Ag content was increased to 40 wt% (40FSP), while both Ag clusters (1–2 nm) and relatively large Ag particles (~ 10 nm) were observed in the case of 10IMP.

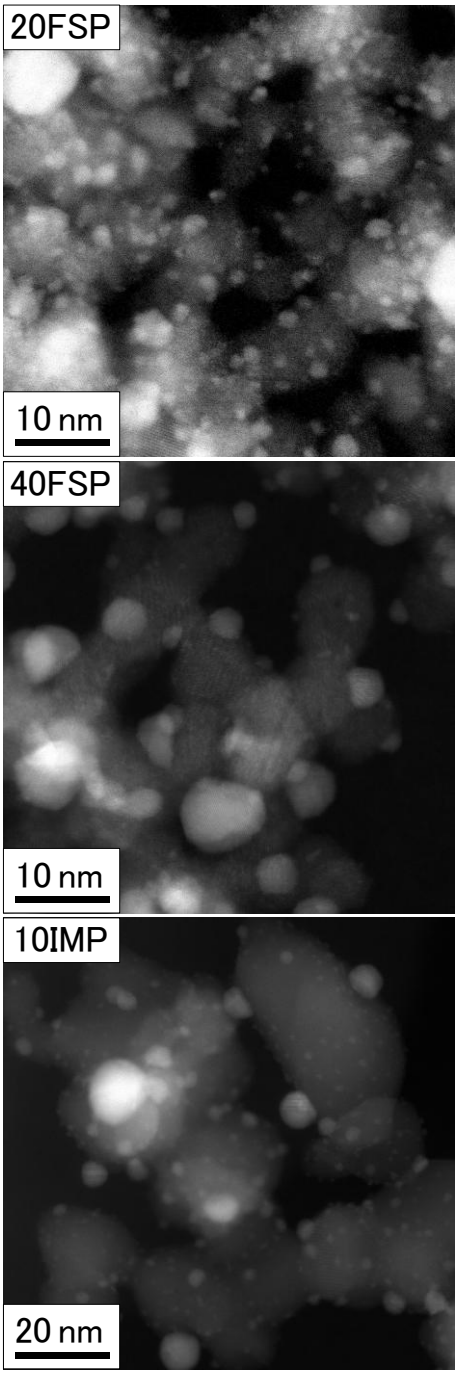

Figure 5 HAADF-STEM images of 20FSP, 40FSP, and 10IMP.

Ag-particle size was quantified by measuring at least 500 particles for each sample. Figure 6 shows the volume-based size distributions of the Ag particles in the *m*FSP and 10IMP catalysts. While small Ag clusters (≤ 3 nm) appear to dominate at $m \leq 20$ wt%, the fraction of relatively large Ag particles (3–10 nm) was observed to gradually increase with increasing Ag content in the *m*FSP catalysts. In contrast, the

wet-prepared 10IMP catalyst exhibited a bimodal Ag size distribution consistent with Ag clusters (≤ 3 nm) and large particles. The fraction of Ag clusters in 10IMP (41%) was comparable to that in 30FSP (49%), although 30FSP contains three-times less Ag than 10IMP, which indicates that the flame-induced Ag–TiO_2 interactions stabilize small Ag clusters. The existence of Ag clusters in the *m*FSP samples is attributable to the abundance of ROS (Fig. 2) ascribable to the large surface area of Ag. In contrast, 10IMP contains less ROS than *m*FSP despite containing Ag clusters. Furthermore, the ROS in the *m*FSP catalysts are regenerated by exposure to O_2, which is behavior that 10IMP is not endowed with. Therefore, the formation of ROS as well as catalytic activity is not only influenced by Ag particle size but also by other properties.

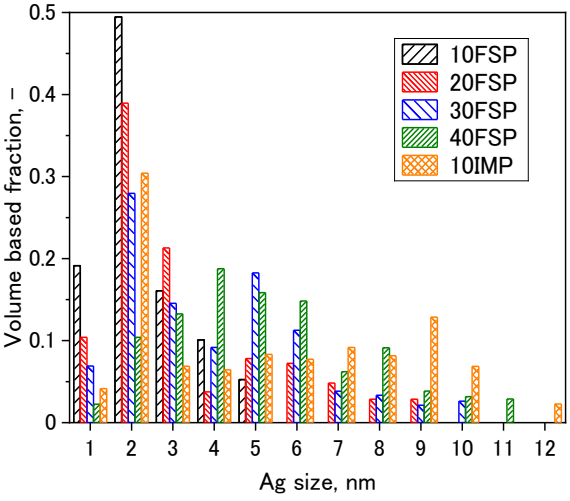

Figure 6 Size distributions of *m*FSP (*m* = 10−40 wt%) and 10IMP

As discussed in the Introduction, the Ag oxidation state plays an important role in determining the activity of a Ag catalyst. Oxidation states were evaluated using XPS and AES. Ag^0 and Ag^+ have XPS peak that are difficult to distinguish because they differ by only 0−0.3 eV. Consequently, we determined the Ag oxidation state from the Auger parameter α (= $E_B + E_k$, where E_B and E_k are the XPS-determined binding energy and AES-determined kinetic energy, respectively).

Figure 6 shows Ag 3d XPS and Ag AES spectra of the *m*FSP (*m* = 10–40 wt%) and 10IMP. The AES and XPS peak locations were corrected by setting the Ag 3d XPS peak to 382.2 eV (Fig. 6a). In this case, 10IMP exhibited an Ag $N_4M_{45}M_{45}$ Auger peak at 357.7 eV, while the *m*FSP exhibited peaks in the 355–356 eV range regardless of Ag content. The Ag $N_4M_{45}M_{45}$ Auger peaks of metallic Ag and Ag_2O are located at 357.8 and 355.9 eV, respectively (dotted lines in Fig. 6b), when the Ag $3d_{5/2}$ XPS peak is set to 382.2 eV because metallic Ag [30] and Ag_2O [31] have α values of 726 and 724 eV, respectively. Consequently, the Ag in 10IMP is in its metallic oxidation state, whereas *m*FSP has a similar Ag oxidation state to Ag_2O. The kinetic energies of *m*FSP (355–356 eV) are slightly lower than those reported in the literature for Ag_2O (355.9 eV). Kaushik [32] reported that the $N_4M_{45}M_{45}$ Auger peaks of Ag^+ vary between 355 and 356 eV, depending on the compound (e.g., Ag_2CO_3, Ag_2SO_4). Therefore, we conclude that Ag exists in the form of Ag^+ in *m*FSP, with a binding state different to that of Ag_2O. The superior CO oxidation activities of the FSP-prepared catalysts are possibly ascribable to their unique oxidation states.

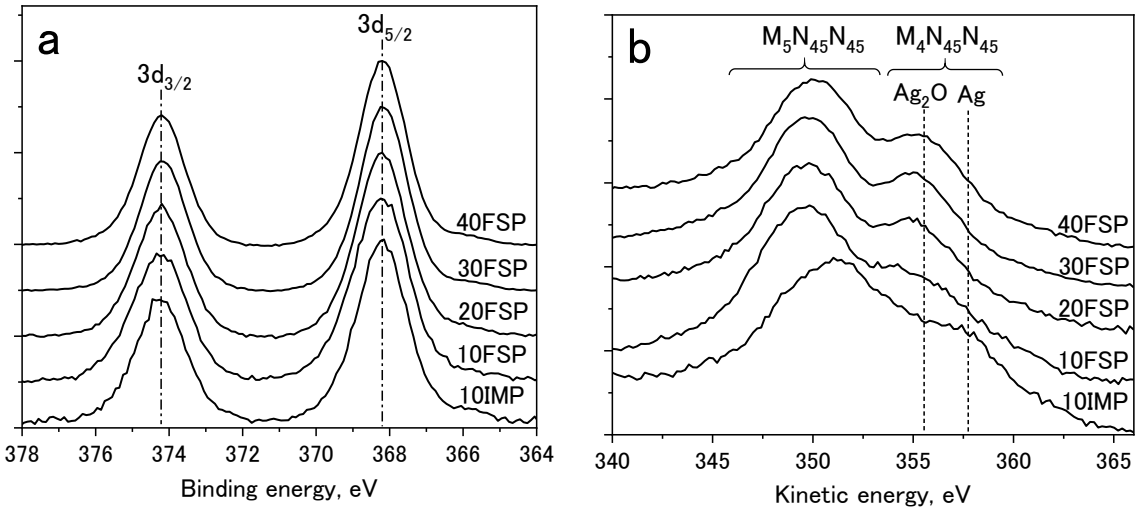

Figure 6 (a) Ag 3d XPS spectra and (b) Ag AES spectra of *m*FSP (*m* = 10−40 wt%) and 10IMP.

The oxidation states of the Ti in the *m*FSP samples also differ from that in 10IMP. Figure 7a shows the Ti 2p XPS spectra of *m*FSP and 10IMP. The spectrum of 10IMP exhibits two peaks at 458.8 and 464.6 eV that correspond to the Ti $2p_{1/2}$ and $2p_{3/2}$ binding energies of Ti^{4+}, respectively. [33] Ti^{3+} and Ti^{2+} exhibit Ti $2p_{1/2}$ binding energies that are 1.5 and 3.5 eV lower than that of Ti^{4+}, respectively (dotted lines in Fig. 7). [34] Accordingly, the Ti in the TiO_2 in 10IMP exists predominantly in its 4+ state, consistent with the PXRD data (Fig. 3).

The *m*FSP samples exhibit Ti $2p_{1/2}$ peaks that lie between those of Ti^{3+} and Ti^{4+}, and gradually shifted to lower energies with increasing Ag content, which indicates that the Ti^{3+} fraction increases with increasing Ag content. According to the PXRD patterns (Fig. 3), *m*FSP consists of TiO_2 and TiO_x ($x < 2$); accordingly the Ti in the TiO_x exists in the 3+ oxidation, consistent with the electron paramagnetic resonance data previously reported by us [17]. Indeed, the higher Ti^{3+} fraction in response to the Ag content is consistent with a higher TiO_x fraction, as confirmed by PXRD. Hence, Ti^{3+} species are formed by interactions involving titanium oxides because the Ti^{3+} fraction is related to the Ag content; these interactions are presumed to be ascribable to electron transfer from the titanium oxides to Ag that lead to the formation of both Ti^{3+} and cationic Ag species. The high catalytic activities of the *m*FSP catalysts are attributable to these interactions, which are induced during flame synthesis, because these interactions are only observed for the FSP-made catalysts.

Interactional stability in the flame-made Ag-TiO_2 was examined based on the oxidation states of Ag and Ti in 20FSP following reaction. Figure 8 shows the Ag AES and Ti 2p XPS spectra of 20FSP before and after three reaction cycles. The AES (Fig. 8a) and Ag 3d XPS (Fig. S3) spectra are unchanged following the reaction. In addition, the Ti 2p XPS spectra acquired before and after the reaction are also

identical, which indicates that the fraction of Ti^{3+} species in the 20FSP catalyst does not change during the reaction. The Ti XPS spectra before and after the reaction are consistent with the intensities of the TiO_x peaks in the PXRD pattern acquired after the reaction (Fig. 4). As a result, the interactions formed between the titanium oxides and Ag remain following the reaction. This interactional stability is consistent with the observed durability of the catalyst.

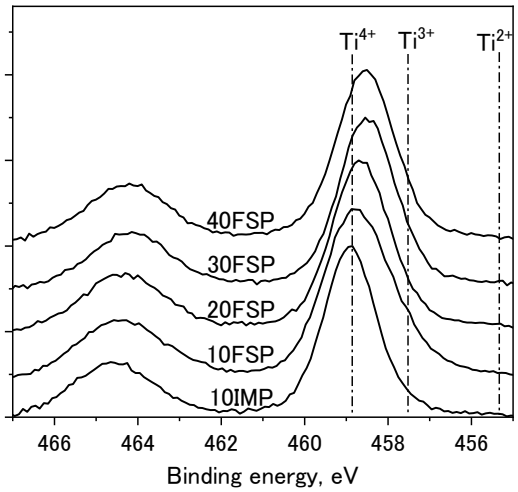

Figure 7 Ti 2p XPS spectra of *m*FSP (*m* = 10−40 wt%) and 10IMP.

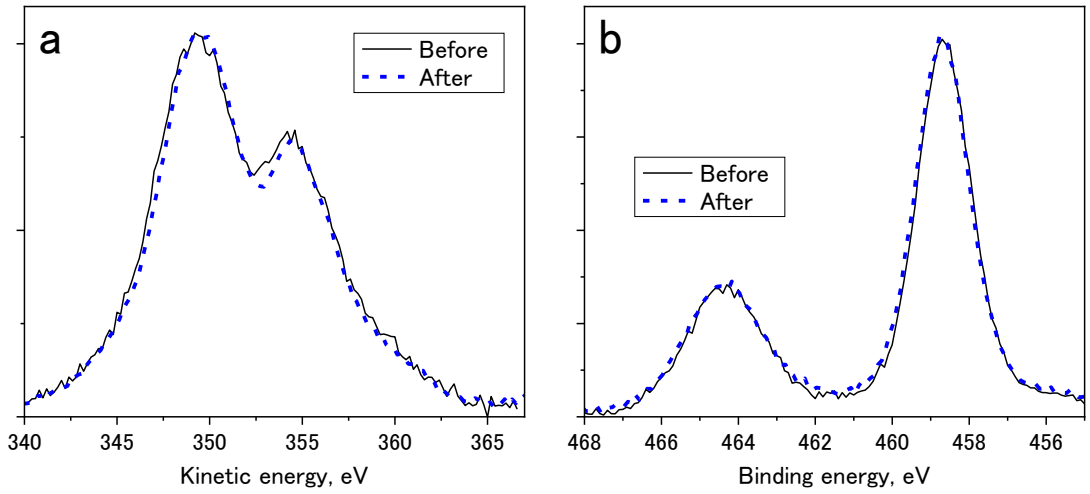

Figure 8 (a) Ag AES and (b) Ti 2p XPS spectra of 20FSP before and after three reaction cycles.

4. Conclusions

In this study, *m* wt% Ag catalysts supported on titanium oxides (*m*FSP) were synthesized by flame spray pyrolysis (FSP). The *m*FSP catalysts exhibited superior catalytic activities for CO oxidation compared to a conventional wet-made catalyst (10IMP). The FSP-based catalysts, particularly 20FSP and 30FSP, showed outstanding CO-oxidation activities, even at room temperature. Moreover, 20FSP demonstrated excellent durability over multiple reaction cycles. The high activity of 20FSP is attributable to the abundant reactive oxygen species (ROS) produced in the catalyst, which can be regenerated by exposure to O_2.

Material characterization revealed that flame synthesis induces unique interactions between Ag and the titanium oxides that stabilize small Ag clusters (< 3 nm) and lead to the formation of sub-stoichiometric TiO_x ($x > 2$) and cationic Ag species. Importantly, Ag particle size and the oxidation states of Ag and Ti in 20FSP remained unchanged after repeated CO oxidation cycles, confirming that the abovementioned interactions are stable. These interactions are considered crucial for enhancing catalytic performance because they are only observed in the FSP-prepared catalysts and not in their wet-impregnated counterparts. Therefore, FSP offers a promising route for fabricating highly active and durable Ag-based oxidation catalysts.

Acknowledgments

The authors gratefully acknowledge the generous support of JSPS KAKENHI (22K14534), Hosokawa Powder Technology Foundation (20109) and Paloma Environmental technology Development Foundation. Electron microscopy measurements were supported by "ARIM Project of the Ministry of Education, Culture, Sports, Science and Technology, Japan (MEXT), Grant No. JPMXP1223OS0036" at the Research Center for Ultra-High Voltage Electron Microscopy (Nanotechnology Open Facilities) in Osaka University. The XPS measurements were supported by MEXT Project for promoting public utilization of advanced research infrastructure (Program for supporting construction of core facilities) Grant Number JPMXS0440300023.

References

[1] L.F. Liotta, Catalytic oxidation of volatile organic compounds on supported noble metals, Appl. Catal. B-Environ., 100 (2010) 403-412.
[2] C. He, J. Cheng, X. Zhang, M. Douthwaite, S. Pattisson, Z. Hao, Recent advances in the catalytic oxidation of volatile organic compounds: a review based on pollutant sorts and sources, Chem. Rev., 119 (2019) 4471-4568.
[3] L. Nie, J. Yu, M. Jaroniec, F.F. Tao, Room-temperature catalytic oxidation of formaldehyde on catalysts, Catal. Sci. Technol., 6 (2016) 3649-3669.
[4] M. Haruta, Gold as a novel catalyst in the 21st century: Preparation, working mechanism and applications, Gold Bull., 37 (2004) 27-36.
[5] K.i. Shimizu, K. Sawabe, A. Satsuma, Self-Regenerative Silver Nanocluster Catalyst for CO Oxidation, ChemCatChem, 3 (2011) 1290-1293.
[6] M. Lamoth, M. Plodinec, L. Scharfenberg, S. Wrabetz, F. Girgsdies, T. Jones, F. Rosowski, R. Horn, R. Schlögl, E. Frei, Supported Ag nanoparticles and clusters for CO oxidation: size effects and influence of the silver–oxygen interactions, ACS applied nano materials, 2 (2019) 2909-2920.
[7] V.V. Dutov, G. Mamontov, V. Zaikovskii, L. Liotta, O. Vodyankina, Low-temperature CO oxidation over Ag/SiO2 catalysts: Effect of OH/Ag ratio, Appl. Catal. B-Environ., 221 (2018) 598-609.
[8] V. Dutov, G. Mamontov, V. Zaikovskii, O. Vodyankina, The effect of support pretreatment on activity of Ag/SiO2 catalysts in low-temperature CO oxidation, Catal. Today, 278 (2016) 150-156.
[9] Z. Qu, F. Yu, X. Zhang, Y. Wang, J. Gao, Support effects on the structure and catalytic activity of mesoporous Ag/CeO2 catalysts for CO oxidation, Chem. Eng. J., 229 (2013) 522-532.
[10] S. Chang, M. Li, Q. Hua, L. Zhang, Y. Ma, B. Ye, W. Huang, Shape-dependent interplay between oxygen vacancies and Ag–CeO2 interaction in Ag/CeO2 catalysts and their influence on the catalytic

activity, J. Catal., 293 (2012) 195-204.
[11] X. Zhang, Z. Qu, X. Li, M. Wen, X. Quan, D. Ma, J. Wu, Studies of silver species for low-temperature CO oxidation on Ag/SiO2 catalysts, Separation and purification technology, 72 (2010) 395-400.
[12] Z. Qu, M. Cheng, W. Huang, X. Bao, Formation of subsurface oxygen species and its high activity toward CO oxidation over silver catalysts, J. Catal., 229 (2005) 446-458.
[13] X. Zhang, Y. Yang, L. Song, Y. Wang, C. He, Z. Wang, L. Cui, High and stable catalytic activity of Ag/Fe2O3 catalysts derived from MOFs for CO oxidation, Molecular Catalysis, 447 (2018) 80-89.
[14] T. Tamura, J. Ohyama, K. Sawabe, A. Satsuma, Enhanced CO oxidation by reversible structural variation of supported Ag nanoparticle catalyst from single to twin by CO treatment, Catal. Today, 411 (2023) 113814.
[15] L. Ma, D. Wang, J. Li, B. Bai, L. Fu, Y. Li, Ag/CeO2 nanospheres: Efficient catalysts for formaldehyde oxidation, Appl. Catal. B-Environ., 148 (2014) 36-43.
[16] J. Sun, D. Ma, H. Zhang, X. Liu, X. Han, X. Bao, G. Weinberg, N. Pfänder, D. Su, Toward monodispersed silver nanoparticles with unusual thermal stability, J. Am. Chem. Soc., 128 (2006) 15756-15764.
[17] K. Fujiwara, Y. Deligiannakis, C.G. Skoutelis, S.E. Pratsinis, Visible-light active black TiO_2-Ag/TiO_x particles, Appl. Catal. B-Environ., 154 (2014) 9-15.
[18] K. Fujiwara, K. Okuyama, S.E. Pratsinis, Metal–support interactions in catalysts for environmental remediation, Environ. Sci. Nano, 4 (2017) 2076-2092.
[19] R. Mueller, L. Madler, S.E. Pratsinis, Nanoparticle synthesis at high production rates by flame spray pyrolysis, Chem. Eng. Sci., 58 (2003) 1969-1976.
[20] K. Wegner, B. Schimmoeller, B. Thiebaut, C. Fernandez, T.N. Rao, Pilot Plants for Industrial Nanoparticle Production by Flame Spray Pyrolysis, KONA Powder Part. J., 29 (2011) 251-265.
[21] K. Fujiwara, S.E. Pratsinis, Single Pd atoms on TiO_2 dominate photocatalytic NO_x removal, Appl. Catal. B-Environ., 226 (2018) 127-134.
[22] K. Fujiwara, S.E. Pratsinis, Atomically dispersed Pd on nanostructured TiO_2 for NO removal by solar light, AIChE J., 63 (2017) 139-146.
[23] S. Ding, H.-A. Chen, O. Mekasuwandumrong, M.J. Hülsey, X. Fu, Q. He, J. Panpranot, C.-M. Yang, N. Yan, High-temperature flame spray pyrolysis induced stabilization of Pt single-atom catalysts, Appl. Catal. B-Environ., 281 (2021) 119471.
[24] K. Fujiwara, T. Akutsu, M. Nishijima, S. Tada, Highly dispersed Zn Sites on ZrO2 by Flame Spray Pyrolysis for CO2 hydrogenation to methanol, Top. Catal., 66 (2023) 1492-1502.
[25] M. Kondo, S. Tada, T. Shioiri, H. Nakajima, M. Nishijima, T. Honma, K. Fujiwara, Aerobic oxidative coupling of 2-naphthols catalyzed by flame-made VO_x/t-ZrO_2: Effect of metal oxide support and VO_x content on catalytic activity, Appl. Catal. A-Gen., 676 (2024) 119638.
[26] J.-H. Liu, A.-Q. Wang, Y.-S. Chi, H.-P. Lin, C.-Y. Mou, Synergistic effect in an Au− Ag alloy nanocatalyst: CO oxidation, J. Phys. Chem. B, 109 (2005) 40-43.
[27] A. Sandoval, A. Aguilar, C. Louis, A. Traverse, R. Zanella, Bimetallic Au–Ag/TiO2 catalyst prepared by deposition–precipitation: High activity and stability in CO oxidation, J. Catal., 281 (2011) 40-49.
[28] S.R. Seyedmonir, D.E. Strohmayer, G.L. Geoffroy, M.A. Vannice, H.W. Young, J.W. Linowski, Characterization of supported silver catalysts: I. Adsorption of O2, H2, N2O, and the H2-titration of adsorbed oxygen on well-dispersed Ag on TiO2, J. Catal., 87 (1984) 424-436.
[29] K.B. Riad, P.M. Wood-Adams, K. Wegner, Flame-made TiO_2 (B), Mater. Res. Bull., 106 (2018) 276-281.

[30] C.J. Powell, Recommended Auger parameters for 42 elemental solids, Journal of Electron Spectroscopy and Related Phenomena, 185 (2012) 1-3.
[31] S. Bera, P. Gangopadhyay, K. Nair, B. Panigrahi, S. Narasimhan, Electron spectroscopic analysis of silver nanoparticles in a soda-glass matrix, Journal of electron spectroscopy and related phenomena, 152 (2006) 91-95.
[32] V.K. Kaushik, XPS core level spectra and Auger parameters for some silver compounds, Journal of Electron Spectroscopy and Related Phenomena, 56 (1991) 273-277.
[33] M.C. Biesinger, L.W. Lau, A.R. Gerson, R.S.C. Smart, Resolving surface chemical states in XPS analysis of first row transition metals, oxides and hydroxides: Sc, Ti, V, Cu and Zn, Appl. Surf. Sci., 257 (2010) 887-898.
[34] A.F. Carley, P.R. Chalker, J.C. Riviere, M.W. Roberts, The identification and characterisation of mixed oxidation states at oxidised titanium surfaces by analysis of X-ray photoelectron spectra, J. Chem. Soc. Faraday Trans., 83 (1987) 351-370.

Supporting information for

Ag clusters on titanium oxides under metal-support interaction for catalytic oxidation in room temperature

by

Kakeru Fujiwara[1, 2*], Souki Terazawa[2], Masahiko Nishijima[3], Yugo Osaka[4], Takuya Tsujiguchi[4] and Akio Kodama[1]

1. Institute for Frontier Science Initiative, Kanazawa University, Kakuma-machi, Kanazawa, Ishikawa 920-1192, Japan.
2. Department of Chemistry and Chemical Engineering, Yamagata University, 4–3–16 Jonan, Yonezawa, Yamagata 992-8510, Japan.
3. Flexible 3D System Integration Lab, SANKEN, Osaka University, 8–1 Mihogaoka, Ibaraki, Osaka 567-0047, Japan.
4. Faculty of Mechanical Engineering, Institute of Science and Engineering, Kanazawa University, Kakuma-machi, Kanazawa, Ishikawa, 920-1192, Japan.

*Corresponding author: k-fujiwara@staff.kanazawa-u.ac.jp/

Characterization of catalysts

N_2 adsorption

N_2 adsorption was performed using a BELSORP-Mini II (MicrotracBEL Corp.). Before the measurements, the samples were degassed at 150 °C under vacuum at < 1 kPa for 1 h. The specific surface area (SSA, m^2 g^{-1}) was calculated from the amount of adsorbed N_2 on the particle surface at –196 °C by the Brunauer–Emmett–Teller (BET) method.

Powder X-ray diffraction (PXRD)

The PXRD patterns of catalysts were obtained using a diffractometer (Rigaku Miniflex, Cu K_α, 40 kV, 15 mA). The crystallite size of metallic Ag was calculated from the peak at 44° using Scherrer's equation (Equation S1).

$$\text{Crystallite size [nm]} = \frac{K \cdot \lambda}{\beta \cdot \cos\theta} \quad \text{(S1)},$$

where K (= 0.89) is the shape factor, λ (= 0.154 nm) is the X-ray wavelength, β is the line broadening at half the maximum intensity in radians, and θ is the Bragg angle.

Electron Microscopy

The particle morphology was investigated by an ultra-high resolution scanning transmission electron microscope (JEOL JEM-ARM200F) equipped with a spherical aberration corrector for a STEM probe. The sample was dispersed in ethanol (Wako, purity > 99.5%) and the suspension was dropped onto a carbon-coated Cu grid (Ohken shoji Co., NP-C15) to deposit the particles on the microgrid film of the grid. The size distributions of Ag in the catalysts were obtained from TEM images by counting at least 500 particles with the software Image J.

X-ray photoelectron spectroscopy

X-ray photoelectron spectroscopy (XPS) and Auger electron spectroscopy (AES) were performed using an X-ray photoemission spectrometer (JEOL, JPS-9010) equipped with a Mg Kα radiation ($h\nu$ = 1253 eV). The pass energies were set at 20 and 50 eV for XPS and AES, respectively. The samples were mounted on an aluminum plate with adhesive carbon tape, and the diameter of the measured spot was about 1 mm. The base pressure of the system was below 1×10^{-6} Pa. To compensate for the eventual surface charging, built-in electron and argon ion neutralizers were used. The Auger spectra of the samples were also measured using the same instrument.

Experimental results

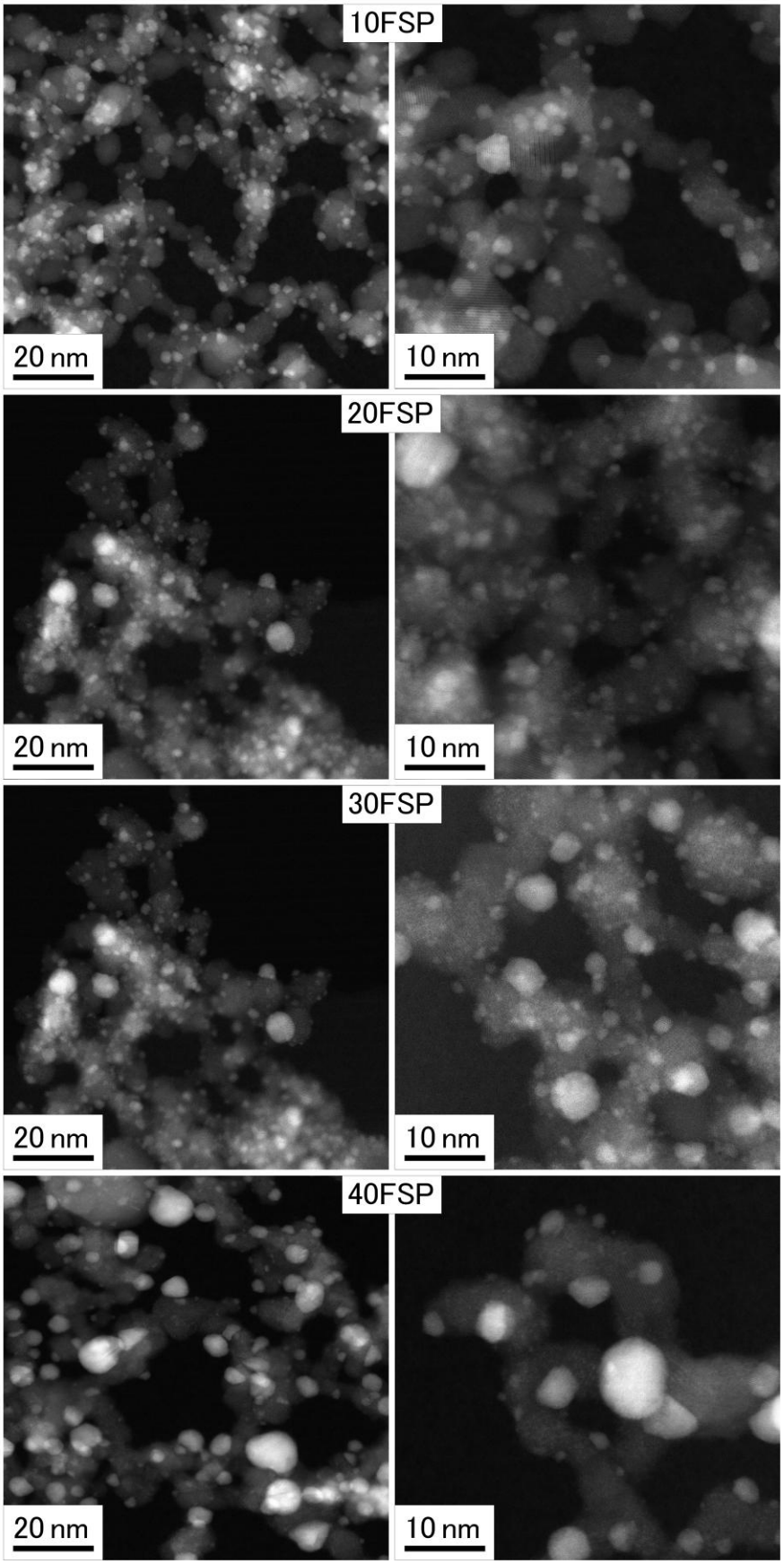

Figure S1 STEM images of FSP-made Ag-TiO_2 (10, 20, 30 and 40FSP).

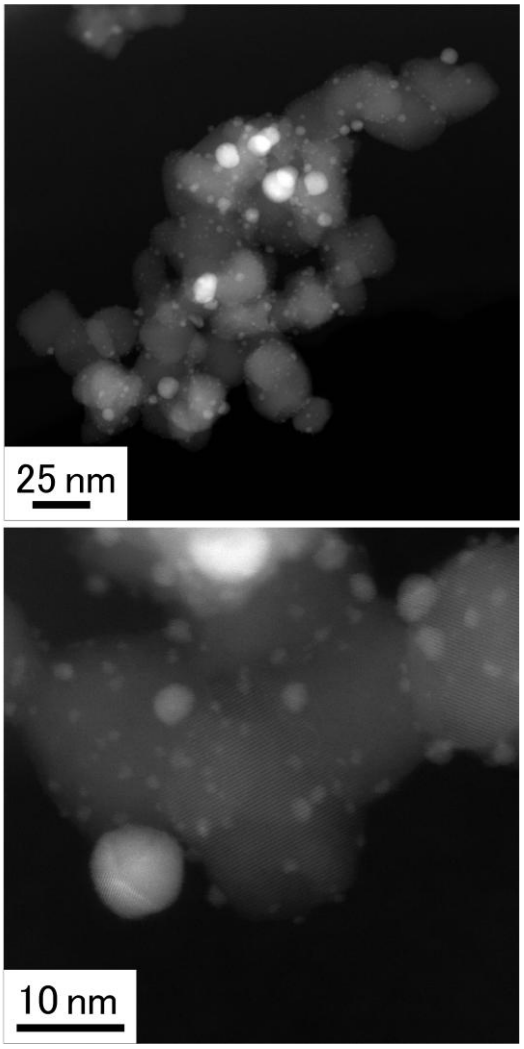

Figure S2 STEM images of 10wt% Ag supported on commercial TiO_2 (Evonik, P25) prepared by impregnation.

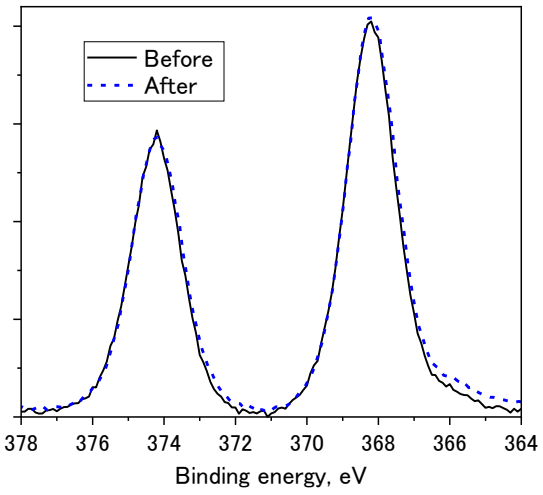

Figure S3 Ag 3d XPS spectra of 20FSP before and after 3 cycles of the reaction tests.